Journal of
Materials Chemistry C

Materials for optical, magnetic and electronic devices

Accepted Manuscript

This article can be cited before page numbers have been issued, to do this please use: Y. Huang, G. Xiao, J. Chen, Y. Shi, Z. Zhang, H. Hu, D. Yuan, Y. Yao, K. Yang and Z. Zeng, *J. Mater. Chem. C*, 2025, DOI: 10.1039/D5TC02503F.

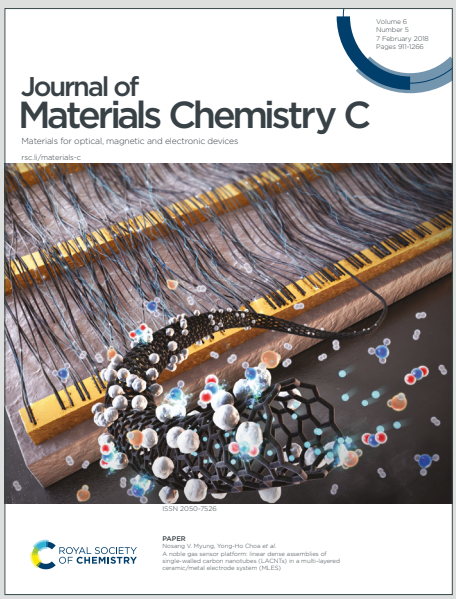

ROYAL SOCIETY OF CHEMISTRY

rsc.li/materials-c

View Article Online
DOI: 10.1039/D5TC02503F

ARTICLE

n-Type Polymer Semiconductors Based on Conformation-Locked π-Extended Bithieno[3,4-c]pyrrole-4,6-dione (BTPD) Acceptor Units for Organic Thermoelectrics

Received 00th January 20xx,
Accepted 00th January 20xx

DOI: 10.1039/x0xx00000x

Yulin Huang,[#a] Guanyu Xiao,[#b] Jie Chen,[#a] Yongqiang Shi,[c] Ziyue Zhang,[d] Huawei Hu,[d] Dafei Yuan,*[b] Yifan Yao,[a] Kun Yang,*[a,e] and Zebing Zeng[a]

Achieving high electrical conductivity in n-type polymers remains a key challenge in organic thermoelectrics. In this study, two conformation-locked, electron-deficient building blocks (BTPD-BTz and BTPD-TTz) were designed by incorporating simple electron-withdrawing bithiazole (BTz) or thiazolothiazole (TTz) units into a classic bithieno[3,4-c]pyrrole-4,6-dione (BTPD) moiety. These building blocks were polymerized via direct C–H arylation polymerization (DArP) to afford two n-type polymers PBTz-TCN and PTTz-TCN, both featuring ultra low-lying LUMO energy levels down to −4.21 eV. Upon n-doping with N-DMBI, PTTz-TCN exhibited a significantly enhanced electrical conductivity of 7.91 S cm^{-1} and a power factor of 0.54 μW m^{-1} K^{-2}—markedly outperforming PBTz-TCN and the benchmark n-type polymer N2200. These results highlight that extending classic electron acceptor units with electron-deficient π-bridges capable of conformational locking is an effective strategy for designing high-performance n-type building blocks for advancing the performance of n-type organic thermoelectric materials.

Introduction

π-Conjugated polymer-based organic thermoelectric materials (OTEs) have received significant attention due to their potential applications in wearable heating and cooling devices, near-room-temperature energy generation, and so on.[1-4] Compared to their inorganic counterparts, OTEs possess unique advantages, including lightweight, intrinsically low thermal conductivity, high solution processability, mechanical flexibility, and great chemical tunability.[5-8] The efficiency of thermoelectric conversion is evaluated by the power factor (PF), which is calculated as $PF = S^2\sigma$, where S is the Seebeck coefficient and σ represents the electrical conductivity. To achieve efficient thermoelectric energy conversion, it is crucial to establish a performance balance between p-type (hole-transporting) and n-type (electron-transporting) polymer thermoelectric materials.[9, 10] However, while substantial progress has been made in the development of high-performance p-type OTEs—with reported σ values exceeding 1000 S cm^{-1} and PFs over 300 μW m^{-1} K^{-2}—n-type counterparts have lagged far behind.[11-14] To date, only a limited number of n-type polymers exhibit σ values above 10 S cm^{-1} and PFs over 10 μW m^{-1} K^{-2}.[15-18] Given that both p-type and n-type materials are required to construct practical thermoelectric devices, the development of high-performance n-type conjugated polymers remains an urgent priority.

A widely adopted strategy for constructing high-performance n-type conjugated polymers is to incorporate electron-deficient building blocks (or called electron acceptors) into the conjugated main chain to lower the frontier molecular orbitals energy levels especially the lowest unoccupied molecular orbital (LUMOs) and thus facilitate electron injection and transport within the devices.[19-21] Classic electron acceptors mainly includes those with strong electron-withdrawing moieties (EWGs) such as imide, amide, cyano,

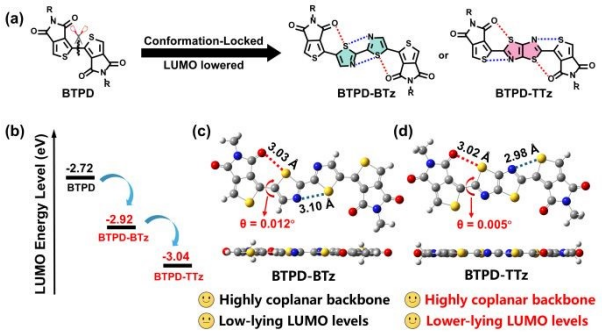

Figure 1. (a) The 'two birds with one stone' design strategy of π-extended BTPD acceptor units in this work; (b) DFT-calculated LUMO energy levels of BTPD-BTz and BTPD-TTz; Top view and side view of (c) BTPD-BTz and (d) BTPD-TTz. The calculations were carried out at the B3LYP/6-31G(d, p) level.

[a] State Key Laboratory of Chemo and Biosensing, College of Chemistry and Chemical Engineering, Hunan University, Changsha 410082, China.
[b] College of Materials Science and Engineering, Hunan University, Changsha 410082, China.
[c] Key Laboratory of Functional Molecular Solids, Ministry of Education, School of Chemistry and Materials Science, Anhui Normal University, Anhui, 241002, China.
[d] State Key Laboratory for Modification of Chemical Fibers and Polymer Materials, College of Materials Science and Engineering, Donghua University, Shanghai 201620, P. R. China
[e] Shenzhen Research Institute, Hunan University, Shenzhen 518000, China
# These authors contributed equally to this work.
Supplementary Information available: [details of any supplementary information available should be included here]. See DOI: 10.1039/x0xx00000x

View Article Online
DOI: 10.1039/D5TC02503H

Kun Yang

Dr Kun Yang received his B.S. degree from University of Science and Technology of China (2011) and Ph.D. degree in Polymer Science from the University of Akron (2017) under the supervision of Prof. Yu Zhu and Prof. Stephen Z. D. Cheng. After a postdoctoral training at Southern University of Science and Technology in the group of Prof. Xugang Guo, he joined Hunan University as an assistant professor in 2022 and now is an associate professor. Dr. Yang's research focuses on organic semiconducting materials and their optoelectronic/magnetic applications.

and boron-nitrogen coordination bonds (B←N),[22-26] as exemplified by naphthalene diimide (NDI),[27] perylene diimide (PDI),[28] bithiophene diimide (BTI),[28] thieno[3,4-c]pyrrole-4,6-dione (TPD),[29] benzodifurandione phenylenevinylene (BDPPV),[30] diketopyrrolopyrrole (DPP),[31] isoindigo (IID),[32] double B←N bridged bipyridine (BNBP),[33] and so on. Among these, imide-functionalized thieno[3,4-c]pyrrole-4,6-dione (TPD) serves as a versatile n-type building block, offering moderate electron-deficiency alongside structural simplicity, intrinsic planarity, and excellent solubility.[34-37] Notably, the bithieno[3,4-c]pyrrole-4,6-dione unit (BTPD)—formed by linking two TPD moieties—exhibits enhanced electron-withdrawing capability with S-O interaction locked planar backbone conformation and is more extensively adopted in n-type polymer development.[38-41] For example, Dong et al. developed a TPD-dimer-based acceptor-acceptor polymer n-type polymer, showing electrical conductivity of 1.3 S cm^{-1} and power factor of 3.0 μW m^{-1} K^{-2} upon doped with Tetrakis(dimethylamino)ethylene (TDAE), both of which are higher than its TPD- and TPD-trimer based counterparts.[42] However, it is still believed that the electron deficiency of BTPD remains unsatisfied as evidenced by the frequently observed ambipolar charge transport behaviors of their resulting polymers in organic field-effect transistors.[43] Therefore, it would be of significance to develop novel BTPD-based highly electron-deficient building blocks with maintained backbone coplanarity to enrich the library of n-type acceptor building blocks and also thermoelectric materials.

Herein, we report the design and synthesis of two n-type polymers based on newly developed electron-deficient building blocks, BTPD-BTz and BTPD-TTz, by incorporating bithiazole (BTz) or thiazolothiazole (TTz) bridge units into the BTPD core (Figure 1a). Introducing BTz and TTz simultaneously lowered the LUMO energy levels of the resulting building blocks and promoted highly planar backbone conformations through intramolecular S···O and S···N noncovalent interactions, thus endowing BTPD-BTz and BTPD-TTz as highly electron-deficient and conformationally rigid n-type building blocks. As in Figure 1b, while density functional theory (DFT) calculations reveal that the LUMO energy levels of BTPD-BTz (-2.92 eV) and BTPD-TTz (-3.04 eV) are substantially reduced compared to the parent BTPD (-2.72 eV), while maintaining excellent backbone planarity through multiple intramolecular noncovalent interactions. Therefore, by employing an environmentally friendly direct arylation polymerization (DArP) method, two n-type polymers, PBTz-TCN and PTTz-TCN, with low-lying LUMO energy levels of -3.93 eV and -4.21 eV, respectively, were prepared and showed ultra deep LUMO energy levels, and highest electrical conductivity (7.91 S cm^{-1}) and power factor (0.54 μW m^{-1} K^{-2}) when doped with 4-(1,3-dimethyl-2,3-dihydro-1H-benzoimidazol-2-yl)-N,N-dimethylaniline (N-DMBI). This work underscores the potential of novel rigid, electron-deficient cores in the molecular design of high-performance n-type organic thermoelectric materials.

Results and discussion

Material synthesis and characterization

The synthetic route for the monomers is illustrated in Scheme 1, with detailed steps provided in the Supporting Information (SI). As depicted in Scheme 1a, the synthesis of bisthiazole-bridged monomer begins with the preparation of amino-substituted thiophene 1 from methyl 2-oxopropanoate and ethyl 2-cyanoacetate through the Gewald reaction.[44] This intermediate was then brominated using the Sandmeyer reaction to produce compound 2.[45] Upon hydrolysis with sodium hydroxide and subsequent dehydration-driven cyclization, anhydride 3 was obtained. Compound 3 was then subjected to imidization with alkyl-linked diamines, yielding compound 4. The final monomer, BTPD-BTz-Br, was synthesized by cross-coupling 4 with 5,5'-bis(trimethylstannyl)-2,2'-bithiazole under standard Pd-catalyzed Stille coupling conditions, followed by bromination with molecular bromine. The synthesis of BTPD-TTz-Br deviates slightly from the route for BTPD-BTz-Br. As shown in Scheme S1 (Supporting Information), compound S1 was first brominated via the Sandmeyer reaction to give S2. The synthesis of S4 followed a similar pathway to compound 4, involving NaOH-assisted hydrolysis, dehydration-driven cyclization, and N-imidization with alkyl-linked diamines. The methyl groups of S4 were then oxidized with selenium dioxide to yield S5, which contained formyl functionalities. However, the condensation reaction between S5 and dithioxamide to form TTz proceeded in low yield, likely due to side reactions induced by the reactive bromo group during cyclization.[46] To address these issues, we modified the synthetic strategy by introducing a key improvement in the final step. In the revised route (Scheme 1b), compound 5 was deaminated with *t*-BuONO in THF to afford 6 in moderate yield.[45] The synthesis of compound 8 followed a similar pathway to compound 4, involving NaOH-assisted hydrolysis, dehydration-driven cyclization, and N-imidization with alkyl-linked diamines. The methyl group of compound 8 was then transformed to intermediate 9 with formyl functionalities using selenium dioxide.[47] Finally, the TTz-bridged monomer BTPD-TTz was successfully synthesized through a double condensation of dithioxamide with 9, followed by bromination with molecular bromine, yielding the electron-deficient acceptor unit BTPD-TTz-Br in 50% yield.

Following the successful synthesis of the two dibrominated monomers, BTPD-BTz-Br and BTPD-TTz-Br, both were subjected to direct arylation polycondensation (DArP) in the presence of Herrmann's catalyst, pivalic acid (PivOH), Copper(I) iodide (CuI) as an additive, and Cs_2CO_3 as the base in toluene, using 3,4-dicyanothiophene as co-polymerized monomer to yield the polymers PBTz-TCN and PTTz-TCN (Scheme 2). Both polymers were purified with standard Soxhlet extraction protocols using methanol, acetone, and hexane to remove the possible small

View Article Online
DOI: 10.1039/D5TC02503F

ARTICLE

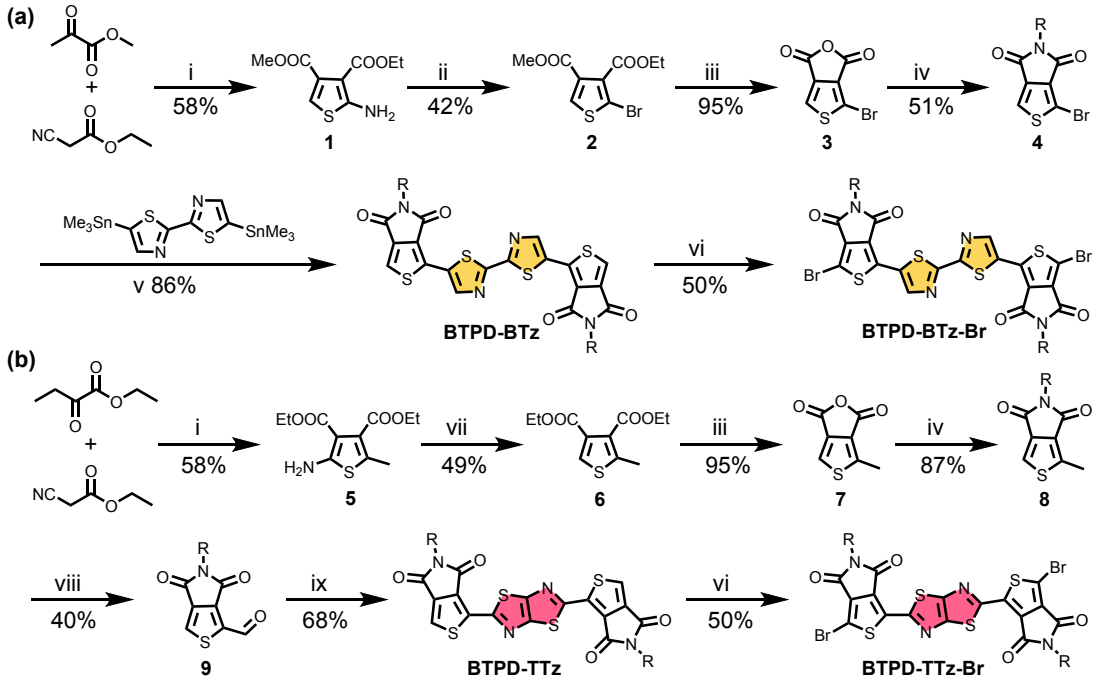

Scheme 1. Synthetic routes of monomers BTPD-BTz-Br and BTPD-TTz-Br. Reagents and conditions: i) S_8, Et_3N, DMF; ii) $NaNO_2$, CuBr, 10% HBr; iii) 1. NaOH (1 M), 2. Ac_2O; iv) 1. 11-(Aminomethyl)tricosane, DMAP, 1,4-dioxane, 2. Ac_2O; v) 5,5'-Bis(trimethylstannyl)-2,2'-bithiazole, $Pd(PPh_3)_4$, toluene, vi) Br_2, $CHCl_3$; vii) *t*-BuONO, THF; viii) SeO_2, Celite, 1,4-dioxane; ix) Ethanebis(thioamide), DMF.

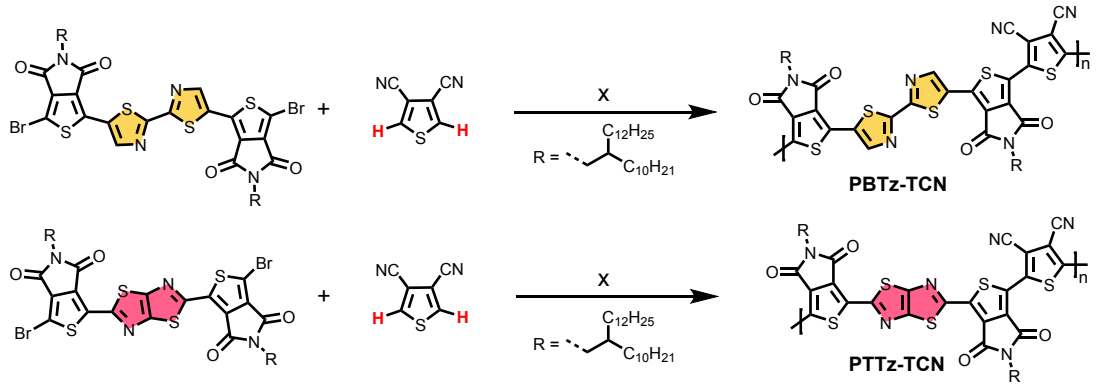

Scheme 2. Synthetic routes of polymers PBTz-TCN and PTTz-TCN. Reagent and conditions: x) Herrmann's cat. $P(o\text{-}MeOPh)_3$, CuI , Cs_2CO_3, PivOH, toluene.

molecular-weight fraction and/or polar impurities whereas the chloroform fractions were collected to give the final polymer products as dark solids in moderate yields of 53 – 77%. Excellent material solubility was observed for both PBTz-TCN and PTTz-TCN in common organic solvents such as chloroform, chlorobenzene and characterized by ^{1}H-NMR spectroscopy (see Figure S8–S33 for the characterization of polymers and related intermediates). High-temperature gel permeation chromatography (HT-GPC) investigation revealed that the polymers possess comparable number-average molecular weights (M_n) and polydispersity indices (PDI) of 29.1 kDa/1.6, 24.3 kDa/2.1 for PBTz-TCN and PTTz-TCN, respectively (Figure S1). Thermogravimetric analysis (TGA) demonstrated excellent thermal stability of two polymers, with rather high decomposition temperatures (5% weight loss) exceeding 300 °C. Differential scanning calorimetry (DSC) measurements further revealed no distinct thermal transition peaks of the polymer solids in the range of 30 – 280 °C, likely suggesting the relatively amorphous nature of these materials in powder state (Figure S2).

Theoretical Calculations

View Article Online
DOI: 10.1039/D5TC02503F

ARTICLE

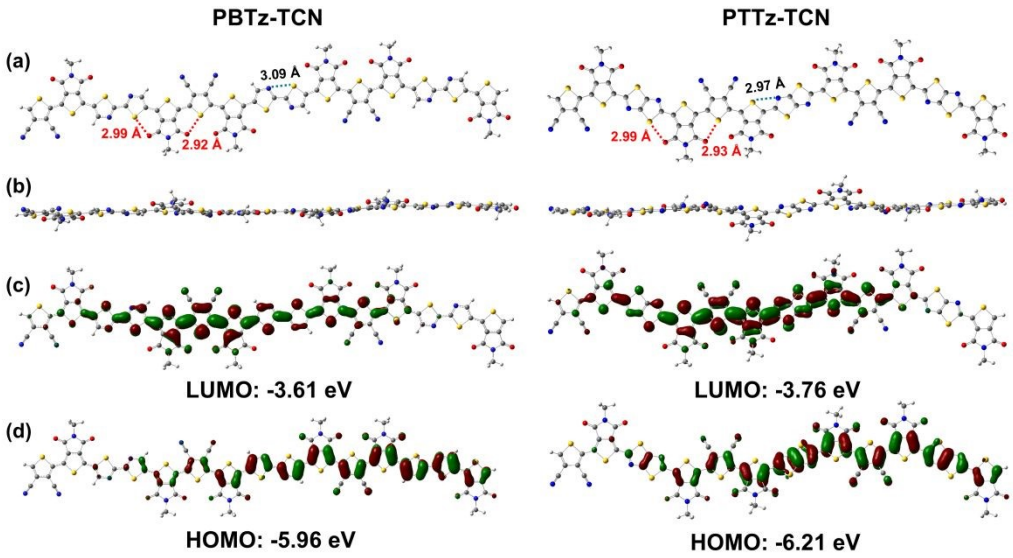

Figure 2. Optimized molecular geometries and electronic structures of polymer PBTz-TCN (left) and PTTz-TCN (right). (a) Top view and (b) side view of optimized ground-state molecular configurations; (c) Calculated LUMO and (d) HOMO profiles for the trimers of two polymers. The DFT calculations were performed at the B3LYP/6-31G(d, p) level.

Density functional theory (DFT) calculations were employed to probe the molecular conformation and electronic structures of the polymers at the B3LYP/6-31G(d, p) level using the trimers of their repeating units with all the alkyl side chains were truncated to methyl groups for computational convenience. As depicted in Figure 2a, the average O···S distances in polymer PBTz-TCN are 2.99 Å (between O atom in TPD unit and S atom in BTz bridge ring) and 2.92 Å (between O atom in TPD moiety and S atom in 3,4-dicyanothiophene unit). Similarly, PTTz-TCN exhibits corresponding O···S distances of 2.99 Å and 2.93 Å. Additionally, the average S···N distances (between S atom in TPD and N atom in TTz bridge ring) are 2.97 Å for PTTz-TCN and 3.09 Å for PBTz-TCN. Clearly, all measured O···S and S···N distances in both polymers are significantly shorter than the sum of their respective van der Waals radii (3.32 Å for S···O and 3.35 Å for S···N), thus confirming the presence of multiple folds of intramolecular noncovalent interactions within their polymer main chains.[48-50] The shorter S···N distance in PTTz-TCN suggests stronger intramolecular interactions, which likely contribute to enhanced backbone rigidity. In addition, both polymers feature a quasi-planar backbone, with average dihedral angles of approximately 4.8° for PBTz-TCN and 5.7° for PTTz-TCN (see Figure S3 for distributions). (detailed dihedral angles in Figure S3). DFT calculations on polymer trimers also reveal lower frontier molecular orbital (FMO) energy levels for PTTz-TCN (HOMO/LUMO: -6.21/-3.76 eV) compared to PBTz-TCN (-5.96/-3.61 eV) (Figure 2c-d). This lowering of FMO levels, resulting from replacing the BTz π-bridge with the more rigid fused-ring TTz unit, is advantageous for efficient n-doping. Furthermore, the rotational freedom of single bonds in the BTz unit may diminish intermolecular interactions.[51] Collectively, the reduced FMO energies are expected to facilitate higher electrical conductivity in relevant (opto)electronic devices.[52]

Photophysical and electrochemical properties

The photophysical properties of polymers PBTz-TCN and PTTz-TCN were investigated in both dilute $CHCl_3$ solution and thin-film states. As shown in Figure 3a, their absorption profiles in solution (300 – 680 nm) are similar. However, the solution maximum absorption wavelength (λ_{max}^{sol}) differs significantly: PBTz-TCN exhibits λ_{max}^{sol} at 538 nm with a shoulder at 574 nm, while PTTz-TCN shows a λ_{max}^{sol} red-shifted by 65 nm to 603 nm, accompanied by a shoulder at 573 nm. The substantial red-shift is likely attributed to the rotatable single bond within the BTz bridge unit, which shortens the effective conjugation length relative to the rigid, ring-fused TTz unit, as well as the high backbone coplanarity of the PTTz-TCN as predicted by DFT calculations.[53] Furthermore, the emergence and intensification of the shoulder peak near 573 nm from PBTz-TCN to PTTz-TCN suggests progressively stronger aggregation tendencies in solution. In the thin-film state, both polymers exhibit absorption spectra similar to their solution profiles but with slight red shifts and broadening. Crucially, the absorption edges were also red-shifted, resulting in optical band gaps (E_g^{opt}) of 1.77 eV for PBTz-TCN and 1.66 eV for PTTz-TCN. Electrochemical properties were assessed by cyclic voltammetry (CV) on thin films (Figure 3b). PBTz-TCN displayed multiple quasi-reversible reduction waves, whereas PTTz-TCN showed a reversible reduction profile. Combining reduction onset potentials with E_g^{opt} yielded HOMO/LUMO energy levels of -5.70/-3.93 eV for PBTz-TCN and -5.88/-4.21 eV for PTTz-TCN (summarized in

View Article Online
DOI: 10.1039/D5TC02503F

ARTICLE

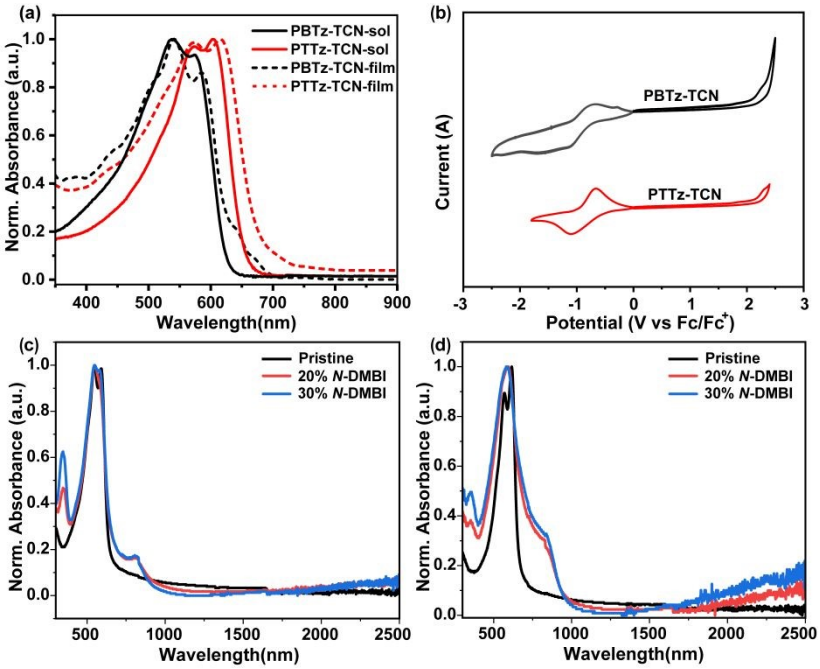

Figure 3. a) UV/Vis absorption spectra of PBTz-TCN and PTTz-TCN in solution and as thin film; b) Cyclic voltammogram of PBTz-TCN and PTTz-TCN as thin film; Normalized UV−vis−NIR absorption spectra of the thin films of (c) PBTz-TCN and (d) PTTz-TCN before and after n-doping with N-DMBI.

Table 1). These low-lying FMO levels, particularly the deeper LUMO of PTTz-TCN compared to both PBTz-TCN and the benchmark n-type polymer N2200,[54] are advantageous for charge transport and n-doping efficiency. Therefore, the significantly lower LUMO level of PTTz-TCN underscores the effectiveness of incorporating the rigid fused-ring TTz unit for lowering the FMOs of TPD-based polymers towards n-type organic semiconductor applications.

Given their favorably deep LUMO energy level, N-DMBI was employed as molecular dopant to explore the n-doping behavior of two polymers. The n-doping efficiency of polymers were estimated with UV−vis−NIR absorption spectroscopy. As shown in Figure 3c and 3d, no prominent absorption peaks above 750 nm were observed in the pristine films. However, upon doping with N-DMBI, two new absorption bands appeared in the near-infrared region, indicating successful n-doping of both polymers. For PTTz-TCN, the new bands around 820 nm and above 2000 nm correspond to the P2 and P1 absorptions of the (bi)polaron.[55] The absorption bands for n-doped PBTz-TCN are similar to those of PTTz-TCN. Notably, PTTz-TCN exhibits a much stronger (bi)polaron absorption under identical doping conditions, suggesting that PTTz-TCN is more efficiently doped than PBTz-TCN, which should be associated with the observed lowering LUMO levels of the TTz-based polymer.

Thermoelectric and Charge Transport Measurement

To evaluate the charge transport properties of polymers, bottom-gate top-contact (BG/TC) configurated field-effect transistors FET devices with PBTz-TCN and PTTz-TCN thin films as the active layers were fabricated and characterized (see the SI for details of device fabrication). As shown in Figure 4a and 4d, both polymers exhibit unipolar n-type transport behaviour, consistent with their low-lying frontier molecular orbital (FMO) levels. Electron mobilities (μ_e) reached 1.97 × 10^{-4} cm^2 V^{-1} s^{-1} for PBTz-TCN and 2.69 × 10^{-3} cm^2 V^{-1} s^{-1} for PTTz-TCN (Figure S4 and table S1). Remarkably, PTTz-TCN demonstrates a >13-fold higher μ_e than PBTz-TCN under identical conditions. This

Table 1. Molecular weights, photophysical and electrochemical properties of the polymers.

Polymer	M_n (KDa)	PDI	λ_{max}^{sol} (nm)	λ_{max}^{film} (nm)	λ_{onset}^{film} (nm)	E_g^{opt} [a] (eV)	E_{red}^{onset} (eV)	LUMO[b] (eV)	HOMO[c] (eV)
PBTz-TCN	29.1	1.6	538	542	700	1.77	-0.87	-3.93	-5.70
PTTz-TCN	24.3	2.1	603	616	742	1.67	-0.59	-4.21	-5.88

[a] $E_g^{opt} = 1240/\lambda_{onset}^{film}$; [b] $E_{LUMO} = -(4.80\ eV + E_{red}^{onset})$; [c] $E_{HOMO} = E_{LUMO} - E_g^{opt}$.

View Article Online
DOI: 10.1039/D5TC02503F

ARTICLE

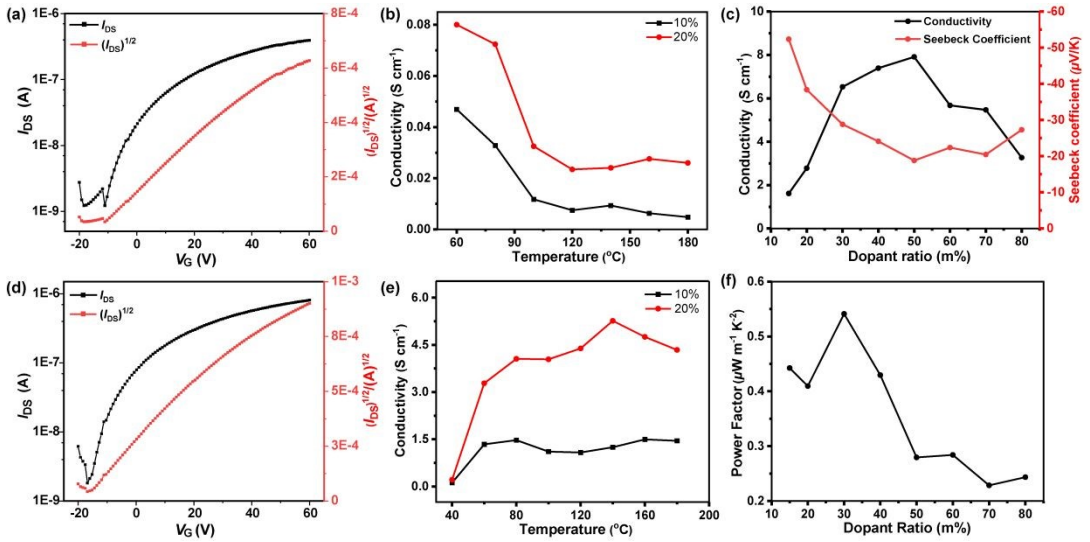

Figure 4. Transfer curves of PBTz-TCN- (a) and PTTz-TCN- (d)-based OFET devices; Electrical conductivity of n-doped PBTz-TCN (b) and PTTz-TCN (e) with various annealing temperature; (c) Electrical conductivity of PTTz-TCN when doped with N-DMBI at different ratios. (f) Power factor of PTTz-TCN when doped with N-DMBI at different molar ratios.

dramatically enhanced mobility is attributed to both the deeper FMO energy levels and the rigid fused-ring TTz bridge-induced high backbone coplanarity, which favors enhanced intermolecular packing in the solid state.

Thermoelectric properties of PBTz-TCN/PTTz-TCN blend films, solution-doped with N-DMBI at varying concentrations, were also measured. Electrical conductivity (σ) was first optimized by annealing the doped polymer films at different temperatures. As shown in Figure 4b, the conductivity of PBTz-TCN consistently decreased as the annealing temperature increased from 60 to 180 °C, regardless of the doping level (10% or 20%). This trend is likely attributed to the increased molecular motion of the flexible BTz unit at elevated temperatures, which might disrupt interchain interactions and thus reduces electrical conductivity.[53] In contrast, PTTz-TCN demonstrated a conductivity exceeding 3 S cm^{-1} at 60 °C with a 20% doping level, significantly outperforming PBTz-TCN (σ ≈ 0.08 S cm^{-1}). Consequently, further thermoelectric characterizations were focused solely on PTTz-TCN. As shown in Figure 4c, the highest electrical conductivity (σ_{max}) of 7.91 S cm^{-1} was achieved for PTTz-TN at a 50% dopant concentration. Moreover, the Seebeck coefficient (S) of PTTz-TCN gradually decreased with increasing dopant levels, consistent with the inverse relationship between Seebeck coefficient and charge carrier concentration. The Seebeck coefficient and PF of the doped films were measured by evaluating the thermovoltage (V_{therm}) across a temperature gradient (ΔT) generated using Peltier elements (see Figure S5). Based on the relation $PF = S^2\sigma$, the maximum power factor of PTTz-TCN was determined to be 0.54 μW m^{-1} K^{-2}. A summary of the thermoelectric properties is provided in Table 2. Notably, the electrical conductivity and power factor values of 7.91 S cm^{-1} and 0.54 μW m^{-1} K^{-2}, respectively, surpass those of benchmark n-type polymer semiconductors such as N2200 and TEG-N2200.[56] These results underscore the strong potential of the BTPD-TTz building block for the development of high-performance n-type organic thermoelectric materials.

Table 2. Electron mobilities and n-type thermoelectric performance parameters of the polymers.

Polymers	μ_e [(a)] (cm^2 V^{-1} s^{-1})	σ [(b)] (S cm^{-1})	S (μV k^{-1})	PF [(c)] (μW m^{-1} k^{-2})
PBTz-TCN	1.97×10^{-4}	0.08 (0.07)	–	–
PTTz-TCN	2.69 ×10^{-3}	7.91 (7.72)	-28.79	0.54 (0.51)

(a) Electron mobility measured from OFET devices; (b) Maximum value with the average values from 5 devices included in parentheses.

Film morphology and microstructure analysis

To investigate the impact of doping on polymer film morphology, atomic force microscopy (AFM) was performed on both pristine and doped films. As shown in Figure 5, the undoped PBTz-TCN film exhibits a smooth surface with a low root-mean-square (RMS) roughness of approximately 1.3 nm. In contrast, the pristine PTTz-TCN film displays a significantly rougher surface with an RMS value of 11.5 nm, likely due to stronger aggregation and/or crystallization tendencies, thus consistent with their optical characterization results. Upon doping with N-DMBI, both polymers show a reduction in RMS roughness, likely suggesting good miscibility between the polymers and the dopant. To further explore the doping effect

on molecular packing, two-dimensional grazing-incidence wide-angle X-ray scattering (2D-GIWAXS) measurements were conducted. As shown in Figure 6, both pristine PBTz-TCN and PTTz-TCN films exhibit similar diffraction features and adopt a predominant face-on orientation, characterized by an out-of-plane (OOP) (010) π-stacking diffraction peak. From the in-plane (IP) (100) and (010) diffraction peaks, the lamellar stacking distance and π–π stacking distance were determined to be 29.22 Å and 3.56 Å for PBTz-TCN, and 30.28 Å and 3.54 Å for PTTz-TCN, respectively. The slightly shorter π–π stacking distance in PTTz-TCN suggests stronger intermolecular interactions, in agreement with its superior electron mobility observed in OFET measurements. In addition, to quantify the crystallinity differences, the crystal coherence lengths (CCLs) of the (100) and (010) peaks were estimated using the Scherrer equation. As summarized in Table S3 (Supporting Information), PTTz-TCN exhibits slightly larger CCLs than PBTz-TCN, indicating higher crystallinity, which is favorable for charge transport. These findings are consistent with the AFM results.

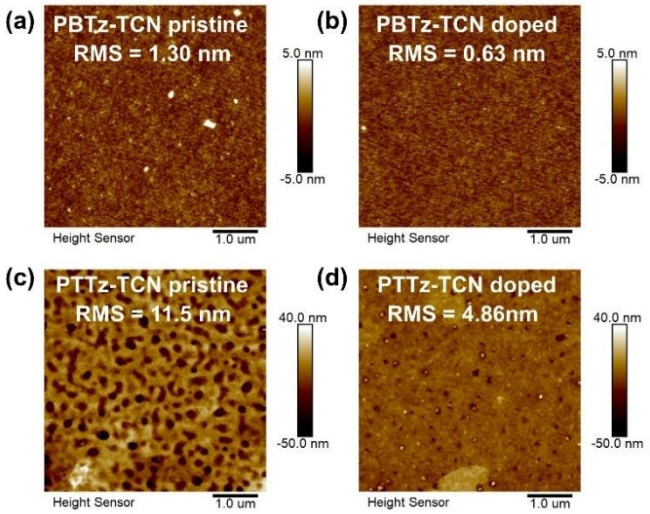

Figure 5. AFM images of PBTz-TCN (a,b) and PTTz-TCN (c,d) films before (a,c) and after (b,d) doping by N-DMBI.

After doping, both polymers show minimal changes in their diffraction patterns and stacking distances in both IP and OOP directions, indicating that their crystalline structures remain largely intact. Since X-ray diffraction primarily reflects changes in crystalline regions and is less sensitive to amorphous domains, this suggests that the dopant molecules are mainly located in the amorphous regions and do not disrupt the crystalline packing. The excellent miscibility of N-DMBI with PTTz-TCN contributes to efficient charge carrier generation and mobility enhancement, ultimately leading to improved n-type thermoelectric performance.

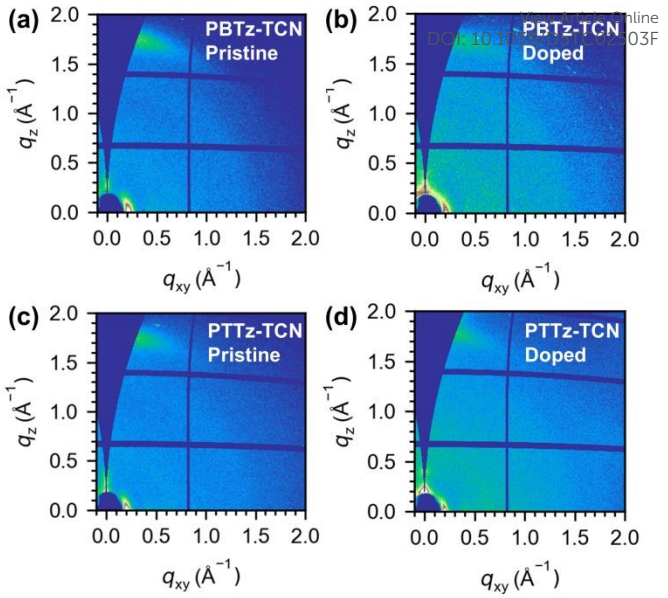

Figure 6. 2D GIWAXS images of PBTz-TCN (a,b) and PTTz-TCN (c,d) films before (a,c) and after (b,d) doping by N-DMBI.

Conclusions

In summary, we have developed two novel BTPD-based n-type building blocks, BTPD-BTz and BTPD-TTz, characterized by high backbone coplanarity, excellent solution processability, and deeper LUMO energy levels than the pristine BTPD moiety. Utilizing these brominated building blocks, we synthesized polymeric semiconductors PBTz-TCN and PTTz-TCN via direct C–H arylation polymerization (DArP) with 3,4-dicyanothiophene. DFT calculations confirmed the presence of intramolecular S···O and S···N conformational locks in both polymers. Electrochemical characterization revealed that PTTz-TCN possesses significantly deeper LUMO levels than PBTz-TCN, achieving an ultralow value of -4.21 eV. Upon doping with N-DMBI, PTTz-TCN demonstrated optimal n-type performance, with electrical conductivity reaching 7.91 S cm^{-1} and power factors up to 0.54 μW m^{-1} K^{-2} – surpassing both PBTz-TCN and the benchmark n-type polymer N2200. This work not only introduces two potent electron-deficient building blocks for unipolar n-type thermoelectrics but also establishes the strategic incorporation of the electron-withdrawing TTz bridge unit as an effective design paradigm for achieving deeper LUMO levels and enhanced thermoelectric performance in organic semiconductors.

Author contributions

Yulin Huang: contributed to the data curation, formal analysis, investigation, visualization, and writing– original draft. Guanyu Xiao: contributed to the data curation, formal analysis, investigation, visualization. Jie Chen: contributed to the data curation, formal analysis, investigation, visualization. Yongqiang Shi: contributed to the GPC measurement. Ziyue Zhang and Huawei Hu: contributed to the GIWAXS characterization. Dafei Yuan: contributed to funding

acquisition, and review and editing. Yifan Yao: contributed to funding acquisition. Kun Yang: contributed to the methodology, resources, validation, funding acquisition, and writing– review and editing. Zebing Zeng: contributed to funding acquisition.

Conflicts of interest

There are no conflicts to declare.

Data availability

The data supporting this article have been included as part of the SI.

Acknowledgements

The authors thank the Special Funds for the Science and Technology Program of Hunan Province (2024RC1027), Guangdong Basic and Applied Basic Research Foundation (2025A1515010687), National Natural Science Foundation of China (52350058, 22375059, 52273174, 22305074), the Natural Science Foundation of Hunan Province (2023JJ10014, 2024JJ4013), We are also grateful to Analytical Instrumentation Center of Hunan University for their support of NMR measurements. The authors also would like to express our gratitude to beamline BL16B1 at Shanghai Synchrotron Radiation Facility (SSRF) for their support during the GIWAXS experiment.

Notes and references

1 Y. Jia, Q. Jiang, H. Sun, P. Liu, D. Hu, Y. Pei, W. Liu, X. Crispin, S. Fabiano, Y. Ma and Y. Cao, *Adv. Mater.*, 2021, **33**, 2102990.
2 Z. Ji, Z. Li, L. Liu, Y. Zou, C.-a. Di and D. Zhu, *Adv. Mater. Technol.*, 2024, **9**, 2302128.
3 S. Masoumi, S. O'Shaughnessy and A. Pakdel, *Nano Energy*, 2022, **92**, 106774.
4 M. Wang, H.-S. Tsai, C. Zhang, C. Wang and S.-H. Ho, *Chin. Chem. Lett.*, 2022, **33**, 2807-2816.
5 W. Zhao, J. Ding, Y. Zou, C.-a. Di and D. Zhu, *Chem. Soc. Rev.*, 2020, **49**, 7210-7228.
6 C.-C. Tseng, K.-C. Wang, P.-S. Lin, C. Chang, L.-L. Yeh, S.-H. Tung, C.-L. Liu and Y.-J. Cheng, *Small*, 2024, **20**.
7 J. Han, E. Tiernan, T. Lee, A. Chiu, P. McGuiggan, N. Adams, J. A. Tomko, P. E. Hopkins, S. M. Thon and J. D. Tovar, *Adv. Mater.*, 2022, **34**, 2201062.
8 S. Zhang, X. Dai, W. Hao, L. Liu, Y. Ma, Y. Zou, J. Zhu and C.-a. Di, *Chin. Chem. Lett.*, 2024, **35**, 109837.
9 L. Tu, H. Wang, X. Li, X. Wang, M. Li, Y. Wang and Y. Shi, *J. Mater. Chem. C*, 2023, **11**, 11905-11911.
10 K. Zhao, Z. Wang, Q.-Y. Wan, J.-C. Zeng, L. Ding, J.-Y. Wang and J. Pei, *Chin. Chem. Lett.*, 2025, **36**, 110339.
11 D. Wang, J. Ding, Y. Ma, C. Xu, Z. Li, X. Zhang, Y. Zhao, Y. Zhao, Y. Di, L. Liu, X. Dai, Y. Zou, B. Kim, F. Zhang, Z. Liu, I. McCulloch, M. Lee, C. Chang, X. Yang, D. Wang, D. Zhang, L.-D. Zhao, C.-a. Di and D. Zhu, *Nature*, 2024, **632**, 528-535.
12 G. Pacchioni, *Nat. Rev. Mater.*, 2024, **9**, 604-604.
13 Y. Gao, Y. Ke, T. Wang, Y. Shi, C. Wang, S. Ding, Y. Wang, Y. Deng, W. Hu and Y. Geng, *Angew. Chem. Int. Ed.*, 2024, **63**, e202402642.
14 Z. Zhang, Y. Sun, X. Shi, X. Yin, D. Liu, E. Wang, J. Liu, Y. Hu and L. Jiang, *Chin. Chem. Lett.*, 2025, **36**, 110786.
15 M. Xiong, X.-Y. Deng, S.-Y. Tian, K.-K. Liu, Y.-H. Fang, J.-R. Wang, Y. Wang, G. Liu, J. Chen, D. R. Villalva, D. Baran, X. Gu and T. Lei, *Nat. Commun.*, 2024, **15**, 4972.
16 X.-Y. Deng, Z. Zhang and T. Lei, *JACS Au*, 2024, **4**, 4066-4083.
17 T. Shen, D. Liu, J. Zhang, Z. Wei and Y. Wang, *Angew. Chem. Int. Ed.*, 2024, **136**, e202409018.
18 L. Zhao, H. Liu, W. Li, Y. Yang, X. He, Z. Zhang, Y. Zhao, Y. Yao, L. Sun and K. Yang, *Angew. Chem. Int. Ed.*, 2025, e202507603.
19 T. Hodsden, K. J. Thorley, J. Panidi, A. Basu, A. V. Marsh, H. Dai, A. J. White, C. Wang, W. Mitchell and F. Glöcklhofer, *Adv. Funct. Mater.*, 2020, **30**, 2000325.
20 G. Zhang, H. Yu, Y. Sun, W. Wang, Y. Zhao, L. Wang, L. Qiu and Y. Ding, *J. Mater. Chem. C*, 2021, **9**, 633-639.
21 J. Chen, J. Yang, Y. Guo and Y. Liu, *Adv. Mater.*, 2022, **34**, 2104325.
22 H. Sun, X. Guo and A. Facchetti, *Chem*, 2020, **6**, 1310-1326.
23 S. Ma, H. Li, W. Wu, S. Gámez‐Valenzuela, R. Ma, Q. Bai, J. Zhong, S. Y. Jeong, Q. Liu and H. Zhang, *Angew. Chem. Int. Ed.*, 2025, **137**, e202423616.
24 H. Zhang, K. Yang, C. Chen, Y. Wang, Z. Zhang, L. Tang, Q. Sun, S. Xue and W. Yang, *Polymer*, 2018, **149**, 266-272.
25 J. Li, M. Liu, K. Yang, Y. Wang, J. Wang, Z. Chen, K. Feng, D. Wang, J. Zhang and Y. Li, *Adv. Energy Mater.*, 2023, **33**, 2213911.
26 D. Yuan, Y. Guo, Y. Zeng, Q. Fan, J. Wang, Y. Yi and X. Zhu, *Angew. Chem. Int. Ed.*, 2019, **58**, 4958-4962.
27 I. Giri, S. Chhetri, M. Mondal, A. B. Dey and R. K. Vijayaraghavan, *Chem. Sci.*, 2024, **15**, 9630-9640.
28 S. Kumagai, H. Ishii, G. Watanabe, C. P. Yu, S. Watanabe, J. Takeya and T. Okamoto, *Acc. Chem. Res.*, 2022, **55**, 660-672.
29 D. Yuan, W. Liu and X. Zhu, *Chem. Soc. Rev.*, 2023, **52**, 3842-3872.
30 Y.-H. Li, J.-Y. Wang and J. Pei, *Acc. Mater. Res.*, 2024, **5**, 1059-1071.
31 R. González-Núñez, G. Martinez, N. R. Avila-Rovelo, K.-I. Hong, A. Ruiz-Carretero and R. P. Ortiz, *J. Mater. Chem. C*, 2024, **12**, 18264-18273.
32 K. Gao, C. Wang, K. Liu and H. Zhang, *Dyes and Pigments*, 2025, **236**, 112685.
33 B. Meng and J. Liu, *Acc. Chem. Res.*, 2024, **57**, 3478-3487.
34 F. Feng, P. Wang, Y. Li and X. Bao, *Mater. Chem. Front.*, 2023, **7**, 3855-3878.
35 C. Dong, S. Deng, B. Meng, J. Liu and L. Wang, *Angew. Chem. Int. Ed.*, 2021, **133**, 16320-16326.
36 S. Deng, C. Dong, J. Liu, B. Meng, J. Hu, Y. Min, H. Tian, J. Liu and L. Wang, *Angew. Chem. Int. Ed.*, 2023, **135**, e202216049.
37 Y. Zou, A. Najari, P. Berrouard, S. Beaupré, B. Réda Aïch, Y. Tao and M. Leclerc, *J. Am. Chem. Soc.*, 2010, **132**, 5330-5331.
38 Y. Jiang, H. Yuan, H. Pan and G. Zhang, *Macromol. Rapid Commun.*, 2025, 2400603.
39 J.-W. Ha, H. J. Park, I.-N. Kang and D.-H. Hwang, *Dyes and Pigments*, 2022, **200**, 110176.
40 Y. Bai, S. Seo, J.-W. Ha, M. Yoon, N. Yang, H. J. Park, S. C. Yoon, C. Lee, D.-H. Hwang and J. Lee, *J. Mater. Chem. C*, 2022, **10**, 18127-18136.
41 S. Zhang, L. Liu, Y. Ma and C.-a. Di, *Chin. Chem. Lett.*, 2024, **35**, 109749.
42 C.-S. Dong, B. Meng, J. Liu and L.-X. Wang, *Chin. J. Polym. Sci.*, 2023, **41**, 108-116.
43 X. Qiao, Q. Wu, H. Wu, J. Zhang and H. Li, *Adv. Funct. Mater.*, 2017, **27**, 1604286.
44 A. Tang, P. Cong, T. Dai, Z. Wang and E. Zhou, *Adv. Mater.*, 2024, **36**, 2300175.
45 P. Berrouard, S. Dufresne, A. Pron, J. Veilleux and M. Leclerc, *J. Org. Chem.*, 2012, **77**, 8167-8173.
46 K. Yamanaka, M. Saito, T. Mikie and I. Osaka, *Bull. Chem. Soc. Jpn.*, 2021, **94**, 2019-2027.

47 D. Wang, J. Li, K. Yang, Y. Wang, S. Y. Jeong, Z. Chen, Q. Liao, B. Li, H. Y. Woo, X. Deng and X. Guo, *ACS Appl. Mater. Interfaces*, 2023, **15**, 9714-9725.
48 J. Li, K. Yang, D. Wang, B. Liu, Y. Wang, S. Y. Jeong, Z. Chen, H. Y. Woo and X. Guo, *Macromolecules*, 2023, **56**, 2339-2347.
49 Y. Shi, Y. Tang, K. Yang, M. Qin, Y. Wang, H. Sun, M. Su, X. Lu, M. Zhou and X. Guo, *J. Mater. Chem. C*, 2019, **7**, 11142-11151.
50 K. Yang, Z. Chen, Y. Wang and X. Guo, *Acc. Mater. Res.*, 2023, **4**, 237-250.
51 Z. G. Zhang and J. Wang, *J. Mater. Chem.*, 2012, **22**, 4178-4187.
52 Z. Chen, J. Li, J. Wang, K. Yang, J. Zhang, Y. Wang, K. Feng, B. Li, Z. Wei and X. Guo, *Angew. Chem. Int. Ed.*, 2022, **61**, e202205315.
53 C. Xue, Y. Tang, S. Liu, H. Feng, S. Li and D. Xia, *New J. Chem.*, 2020, **44**, 13100-13107.
View Article Online
DOI: 10.1039/D5TC02503F
54 F. Chen, Y. Jiang, Y. Sui, J. Zhang, H. Tian, Y. Han, Y. Deng, W. Hu and Y. Geng, *Macromolecules*, 2018, **51**, 8652-8661.
55 X. Yan, M. Xiong, J.-T. Li, S. Zhang, Z. Ahmad, Y. Lu, Z.-Y. Wang, Z.-F. Yao, J.-Y. Wang, X. Gu and T. Lei, *J. Am. Chem. Soc.*, 2019, **141**, 20215-20221.
56 J. Liu, L. Qiu, R. Alessandri, X. Qiu, G. Portale, J. Dong, W. Talsma, G. Ye, A. A. Sengrian, P. C. T. Souza, M. A. Loi, R. C. Chiechi, S. J. Marrink, J. C. Hummelen and L. J. A. Koster, *Adv. Mater.*, 2018, **30**, 1704630.

View Article Online
DOI: 10.1039/D5TC02503F

Data availability Statement

The data supporting this article have been included as part of the SI.